Standing-Wave-Assisted Creation of Nanopillar Arrays with Vertically Integrated Nanogaps for SERS-Active Substrates

Tae Yoon Jeon, Sung-Gyu Park, Dong-Ho Kim, and Shin-Hyun Kim**

An optical method is used to create multi-dimensional metal structures with three distinct periodicities for surface-enhanced Raman scattering (SERS). Periodic arrays of nanopillars are formed by phase-shift interference lithography on sub-micrometer length scales. With the help of a standing wave, each nanopillar is made to be a disk-stacking structure consisting of a series of 20-nm-thick metal nanogaps; the nanopillars consequently resemble a pagoda. The vertically integrated metal nanogaps of the metal-deposited pagoda-like nanopillars enable strong localization of an electromagnetic field and effective enhancement of Raman signals for molecules adsorbed on the metal surface. Moreover, the nanopillars are arranged in a regular lattice, which results in a low spatial variation of the SERS intensity and provides high reproducibility in measurements. Arrays of the nanopillars can be further micropatterned to have a periodicity ranging from tens of micrometers to a millimeter by subsequently employing photo-lithography. The nanopillar arrays promote the wetting of sample fluids, which enables the selective confinement of fluids on the array regions of the micropatterns without spreading. Consequently, numerous fluid samples can be separately deposited, enabling SERS-based analysis of multiple samples using a single substrate.

1. Introduction

Surface-enhanced Raman scattering (SERS) can significantly intensify the Raman signal of molecules absorbed on a metal surface; it has been used to detect and identify chemicals and biomolecules of an infinitesimal quantity.[1] In SERS, surface plasmons strongly localize electromagnetic (EM) waves on the surface of metallic nanostructures, thereby magnifying the EM field on the surface and dramatically enhancing Raman scattering from adsorbed molecules.[2] Amplification of EM intensity is one of the most important factors in improving the limit of detection (LOD) in SERS analysis. Narrow gaps between metal nanostructures amplify the EM intensity by strongly coupling the EM waves due to charge localization at the gaps, making them appealing for SERS applications.[3] Such nanogaps have been precisely designed by e-beam lithography,[4] atomic layer deposition of metal oxides,[5] and a combination of electron-beam-induced deposition and focused ion beam milling;[6] however, such complex and time-consuming fabrication procedures, along with high production costs, severely restrict their practical use in SERS applications. Although colloidal lithography enables the creation of 2D metal nanogaps over a wide area,[7] it is still difficult to achieve high nanogap density and uniform spatial distribution of the SERS intensity. Such limitations have been partially overcome by employing templates of the natural rib-structures in butterfly wings[8] and rose petals[9] for metal deposition; these natural templates consist of periodic nanogaps in a vertical direction, which provide high nanogap density. Natural templates, however, are not mass-producible and may not be easily integrated into existing fabrication techniques.[10] Although nanogaps can be formed in artificial ridged nanostructures, the depth and maximum number of the ridges are limited, and the array spans only an area of 1 mm^2, restricting their SERS efficiency and practical uses.[11] As a result, there is still intense demand for an economical and reproducible method to create SERS substrates with a high density of metal nanogaps for highly sensitive and practical SERS analysis.

Here, we report a one-step lithographic method to create an array of vertically structured nanopillars for use as a SERS-active substrate. The vertical structure of a single nanopillar consists of a series of nanogaps; we refer to the structure as a "pagoda-like nanopillar." The array of nanopillars is prepared by phase-shift interference lithography to have a periodicity of 0.5 μm. Simultaneously, to vertically integrate the nanogaps, a standing wave is generated by a strongly reflecting incident laser beam at the boundary between a photoresist film and underlying substrate. This leads to the formation of disk-stacking structures with a periodicity of approximately 100 nm along the main axis of the nanopillar. To use the array of nanopillars as a SERS-active substrate, silver is deposited on the surface, producing 20-nm-thick nanogaps on the side wall

T. Y. Jeon, Prof. S.-H Kim
Department of Chemical and Biomolecular Engineering (BK21+ Program)
KAIST, Daejeon 305–701, Korea
E-mail: kim.sh@kaist.ac.kr
Dr. S.-G. Park, Dr. D.-H. Kim
Advanced Functional Thin Films Department
Korea Institute of Materials Science (KIMS)
Changwon, Gyeongnam 641–831, Korea
E-mail: dhkim2@kims.re.kr

DOI: 10.1002/adfm.201501274

© 2015 WILEY-VCH Verlag GmbH & Co. KGaA, Weinheim

of the nanopillars. In each nanogap, the EM field is strongly localized, which enables high enhancement of the Raman signals. In addition, the enhancement can be further improved by increasing the number of stories and tapering the nanopillars to have a cone shape. Moreover, this process results in uniform nanopillars with a low spatial variation of the SERS intensity, thereby providing a reliable SERS substrate. The interference lithography can be further combined with photo-lithography to makes micropatterns of the nanopillar arrays, which enables the SERS analysis of multiple samples on a single substrate.

2. Results and Discussion

2.1. Formation of Pagoda-Like Nanopillars

When a laser beam vertically impinges on a 2D grating with a periodicity comparable or larger than the wavelength of light, the images of the grating are repeatedly produced along the propagation direction of incident light with a periodicity larger than that of the grating; this is known as the Talbot effect.[12] As a result, interference lithography only produces regular structures on the length scale of the grating, which is typically several hundred nanometers in both lateral and propagation directions; the resulting structures are consequently inappropriate to be used as templates for metal deposition to form nanogaps for SERS . To integrate a high density of nanogaps, we further tailored the surface of the periodic structure to possess periodic gaps at a length scale of 100 nm by forming a partial standing wave within the photoresist film. Periodic gaps of 100 nm provide 20-nm-thick metallic nanogaps after metal deposition; these are able to efficiently amplify the EM field for SERS applications. A standing wave can arise when two waves with the same frequency travelling in opposite directions interfere. To form a standing wave within the photoresist film, we use the reflection of the incident light at the boundary between the photoresist and underlying substrate. The standing wave has a periodicity of $\lambda/2n$, where λ is the wavelength of light and n is the refractive index of the medium. By using a He-Cd laser with λ = 325 nm and a positive photoresist (AZ 5214E) with n = 1.69, we can form a standing wave with a periodicity of 96 nm. The square array of cylindrical posts with a periodicity of 500 nm, made of NOA 68, is used as a diffraction grating; each post has diameter of 200 nm and height of 200 nm. To maintain a consistent distance between the grating and photoresist over a wide area, 20-μm-thick poly(dimethylsulfoxide) (PDMS) film is used as a spacer that also ensures conformal contact. The experimental set-up is schematically illustrated in **Figure 1**a, and the scanning electron microscopy (SEM) image of the diffraction grating is shown in Figure 1b.

Two waves with the same frequency and amplitude travelling in opposite directions form a standing wave through interference. When the amplitudes are not the same, the standing wave becomes incomplete. As the discrepancy of the amplitude increases, so does deviation from the standing wave. To investigate the influence of reflectance on the formation of the standing wave and periodic vertical gaps, we employed two different substrates for photoresist coating: soda-lime glass (n = 1.46) and silicon wafers (n = 3.7). For a normal incident light, the reflection coefficient, r, is determined by the refractive indices of the propagating media, n_1 and n_2, as $r = (n_1 - n_2)/(n_1 + n_2)$ according to the Fresnel equation. For the photoresist AZ 5214E (n = 1.69) on a silicon wafer, r is –0.373 while for the same photoresist on soda-lime glass, r is 0.073. The reflection coefficient indicates the deviation from the standing wave; it is called the standing wave ratio (SWR). SWR = 1 for a pure standing wave, and SWR = 0 for a pure travelling wave. As a result, the partial standing wave formed by the silicon wafer is approximately 5 times closer to a pure standing wave than that formed by soda-lime glass; this makes an apparent contrast in the formation of the disk-stacking structures in each nanopillar.

When soda-lime glass is used as the substrate for a 500-nm-thick photoresist, the surface of each resulting pillar with an average diameter of 330 nm is undulated to have 5 stories with a periodicity of 96 nm and a depth of 35 nm (Figure 1c). We define the depth as the difference between the largest and smallest radii in a single pillar. In contrast, using a silicon wafer, the substrate yields pillars with an increased depth of 60 nm, while retaining the same periodicity (Figure 1d). As a result, the high refractive index of the substrate is a prerequisite for creating the standing wave, thereby undulating the surface with large amplitude and yielding periodic nanogaps in a disk-stacking structure. The influence of the substrates on the formation of the standing wave can be further confirmed by finite-difference time-domain (FDTD) calculations (Figure 1e); we also compared the intensity profile formed without any substrate and with glass and wafer substrates (Figure S1 in the Supporting Information, SI). With both substrates, partial standing wave is formed along the propagation direction; undulation of light intensity is observed in a periodicity of 96 nm, which is in good agreement with the observation. The intensity variation along the propagation direction is much sharper with a silicon substrate than soda-lime glass substrate. The magnified intensity patterns, sectioned from overall profiles, manifest the difference in the intensity variation (Figures 1e); the low-intensity region remains after development because we used a positive photoresist.

2.2. SERS Activity of Pagoda-Like Nanopillars

To create metal nanogaps for SERS, we sputtered silver onto the surface of the pagoda-like structures with 5 stories and prepared with a silicon-wafer substrate, in order to have a gap width of 20 nm, (**Figure 2**a). The sputtering is not highly directional but isotropic relative to electron-beam evaporation, enabling the formation of a continuous silver film on the side walls.[13] We confirmed this by etching the silver film on the top surface of the nanopillars using argon ion-milling and subsequently removing the AZ 5214E polymer by ethanol treatment. This left hollow silver tubes with side walls that were continuously undulated (Figure S2, SI). This isotropic silver deposition reduces the gap width from 40 to 20 nm. For a comparison, we deposited silver on the surface of the nanopillars with 5 stories and prepared with the soda-lime-glass substrate, in order to study the influence of nanogap depth on SERS activity (Figure 2b); the surface undulation becomes indistinct after silver deposition. In addition, we deposited silver on the surface of pillars without undulation to study the importance of the nanogaps (Figure 2c); the diffraction

© 2015 WILEY-VCH Verlag GmbH & Co. KGaA, Weinheim

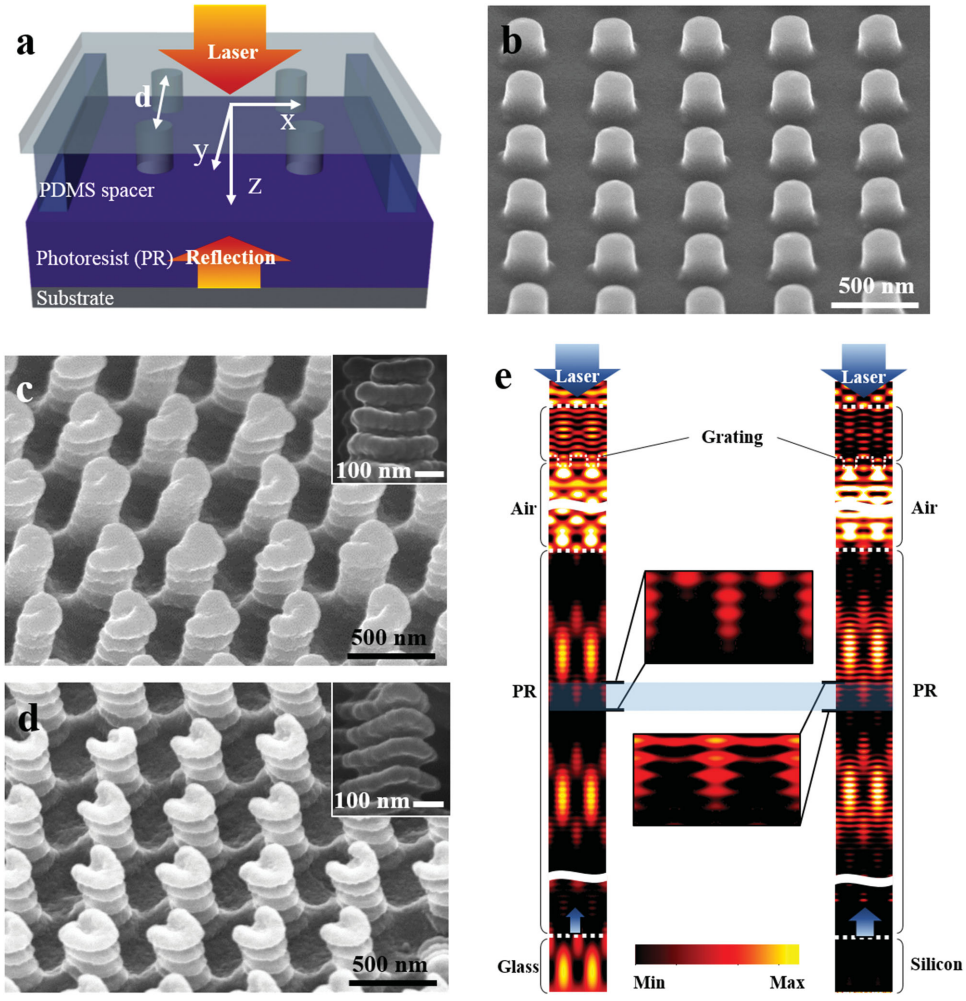

Figure 1. a) Schematic diagram of experimental set-up for phase-shift interference and standing wave formation. *d* represents the grating period. b) SEM image of diffraction grating with 500-nm periodicity. c,d) SEM images of nanopillar arrays with undulating side walls; soda-lime glass (c) and silicon (d) are used as substrates. A side view of a single nanopillar is shown in each of the insets. e) Intensity profiles at the $y = d/2$ plane calculated by the FDTD method for the underlying soda-lime glass (left) and silicon wafer (right). The two images in the middle show representative intensity profiles corresponding to nanopillars in c and d. PR represents the photoresist.

grating is used as a template for this purpose. To evaluate and compare the SERS-activity of these three different structures, we prepared a monolayer of benzenethiol (BT) on the metal surfaces and obtained the Raman spectra using a 633-nm laser with an intensity of 1 mW, spot diameter of 1 μm, and integration time of 5 s; for this, all three structures were immersed in 2-mM BT dispersed in ethanol for 1 h and then rinsed with ethanol. As indicated in Figure 2d, the pagoda-like nanopillars prepared with the silicon wafer exhibited distinct peaks at 994, 1017, 1071, and 1571 cm^{-1} (black spectrum).[14] While the nanopillars prepared with soda-lime glass showed a signal that was approximately four times weaker (red), no Raman signal was observed from the pillar with smooth surface (blue). These data indicate that the metal nanogaps formed on the distinct pagoda-like nanopillars strongly localize the EM field and enhance Raman signal intensity. This is further confirmed with the FDTD calculations (Figure 2e). The electric field is strongly localized at the metallic nanogaps on the side walls at which the maximum electric field intensity ($|E_{Max}|^2$) is enhanced approximately 400 times relative to the incident field.

Because the pagoda-like nanopillars are uniform and form an array, they provide consistent Raman intensity. Independent measurements of the spot position indicated that the spot diameter is larger than 500 nm. As shown in Figure 2f, we mapped the intensity of the Raman signal at 994 cm^{-1} from an area of 1 μm^2 with a 633-nm laser with an intensity of 0.3 mW and integration time of 1 s. Each measurement involved four nanopillars. The coefficient of variation (CV) of Raman intensities from 121 pixels is as small as 14.8%, indicating high uniformity among the nanopillars and providing high reliability for SERS measurement; this is superior to liquid-crystal-based SERS substrates (CV: 21%) and the commercial Klarite SERS substrate (CV: 45%).[15]

2.3. Structural Optimization of Pagoda-Like Nanopillars

To improve the SERS activity of the pagoda-like nanopillars, we increased the number of levels up to 8 by employing a photoresist with a thickness of 800 nm (**Figure 3**a). A distinct

© 2015 WILEY-VCH Verlag GmbH & Co. KGaA, Weinheim

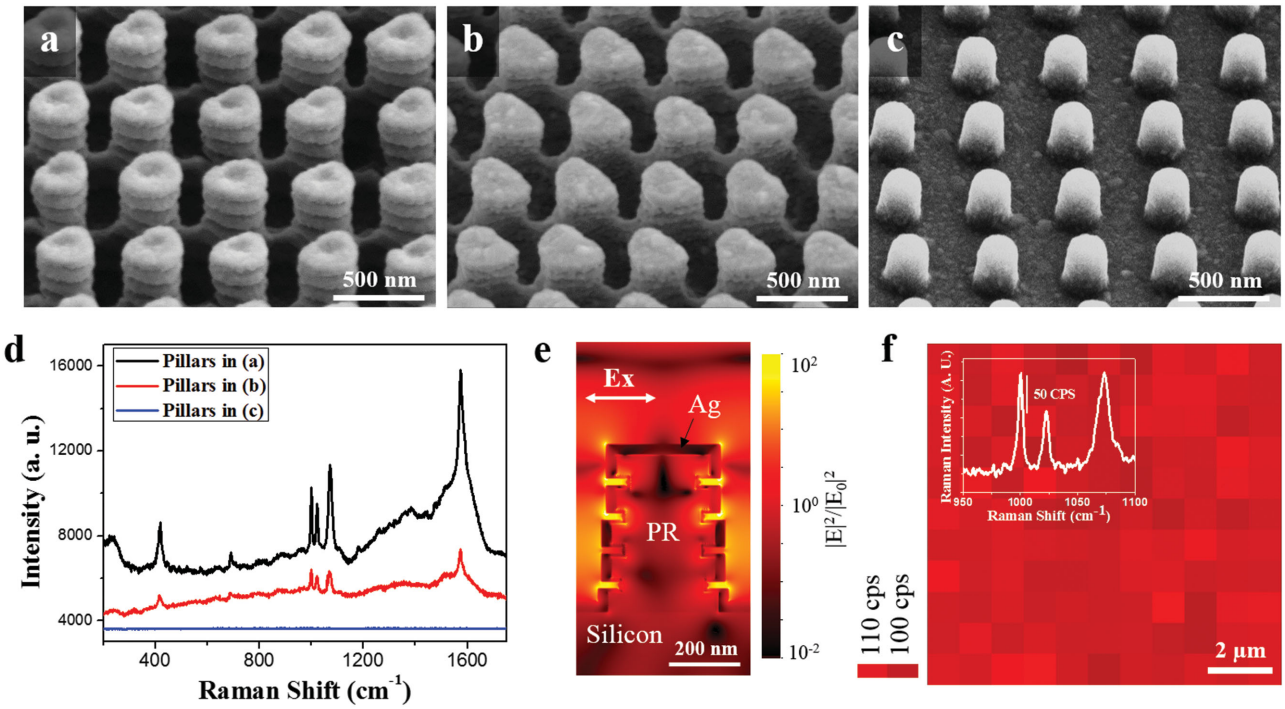

Figure 2. a–c) SEM images of silver-deposited nanopillar arrays, where pillars in a and b are prepared by employing phase-shift interference and a partial standing wave with substrates of silicon wafer (a) and soda-lime glass (b); pillars in c are prepared by replicating the diffraction grating. d) Raman spectra of benzenethiol (BT) molecules adsorbed on the surfaces of three distinct nanopillars in a–c. e) Spatial distribution of the electric field intensity normalized by the electric field of the 633-nm incident light, $|E|^2/|E_0|^2$, in silver-deposited disk-stacking structure. This is calculated by the FDTD method with the geometric dimensions of the nanopillars in (a). EX represents the polarization direction of electric field. f) Map of Raman intensity at 994 cm^{-1} measured from the BT adsorbed on the surface of nanopillars in a, where each measurement covers an area of 1 μm^2 and the map comprises 121 pixels. Coefficient of variation of the intensity is 14.8%.

cylindrical disk was formed for each level (Figure 3b), and this is confirmed by FDTD calculations (Figure 3b, inset), which shows a constant width for the low-intensity region. The nanopillar can be further modified by increasing the laser dose. When the dose is increased from 4.3 to 6.9 J cm^{-2}, the pagoda-like structures become tapered while retaining their number of distinct disk-shaped stories (Figure 3c,d). The larger laser dose more successfully degrades the positive photoresist, which reduces the dimension of the pillar structure. Because the intensity of the interference beam gradually decreases in the photoresist film along the propagation direction, a larger dose leads to a large reduction in the stack radius at the top and small reduction at the bottom, forming tapered nanopillars with distinct levels. This can be verified by FDTD calculations (Figure 3d, inset); with a large laser dose, the width of the low-intensity region gradually decreases from bottom to top. The pagoda-like nanopillars can be arranged periodically over a wide area of 1 cm^2 (Figure 3e), where the regular array of nanopillars causes diffraction colors. The patterned area is limited only by spot size of the laser beam. The array of tapered nanopillars with 8 stories is shown in Figure 3e (and Figure S3, SI). We benchmarked the SERS activity of the straight and tapered nanopillars with 8 stories and a commercially available SERS substrate, and we compared them with that of nanopillars with 5 stories. For this, we formed a monolayer of BT molecules on the surface and obtained the Raman spectra, in the same manner as the nanopillars in Figure 2d. The straight nanopillars with 8 stories exhibited a Raman signal 1.63 times greater than that of the nanopillars with 5 stories (**Figure 4**a,b). The Raman signal was calculated from the average intensity of four characteristic peaks of BT. The tapered nanopaillars with 8 stories had a signal that was approximately 2.4 times greater than that of the nanopillars with 5 stories. In addition, we compared the SERS activity of the pagoda-like nanopillars with the commercial SERS substrate (Klarite SERS substrate) (Figure 4a). The Raman intensity from the tapered nanopillars is approximately 35 times higher than that from the Klarite substrate, thereby enabling the tapered nanopillars to provide much higher sensitivity.

The enhancement of Raman intensity in the non-tapered 8-story nanopillars compared to that in the 5-story nanopillars is attributed to an increased number of hotspots; the number of nanogaps increases from 4 to 7, thereby providing roughly 1.75 times more hotspots in the nanogaps. The tapered nanopillars show higher signal than the non-tapered ones with the same number of nanogaps, in spite of their smaller surface area. We investigated this with FDTD calculations (Figure 4c). When considering all the nanogaps of the tapered and non-tapered nanopillars, the EM field is most strongly coupled at the top nanogap of the tapered structures. This is attributed to the additional coupling effect along the lateral direction. At the top nanogap, a polymer disk with a diameter of 70 nm is surrounded by a silver ring, which can facilitate localization of the EM field under the incident beam whose direction of

© 2015 WILEY-VCH Verlag GmbH & Co. KGaA, Weinheim

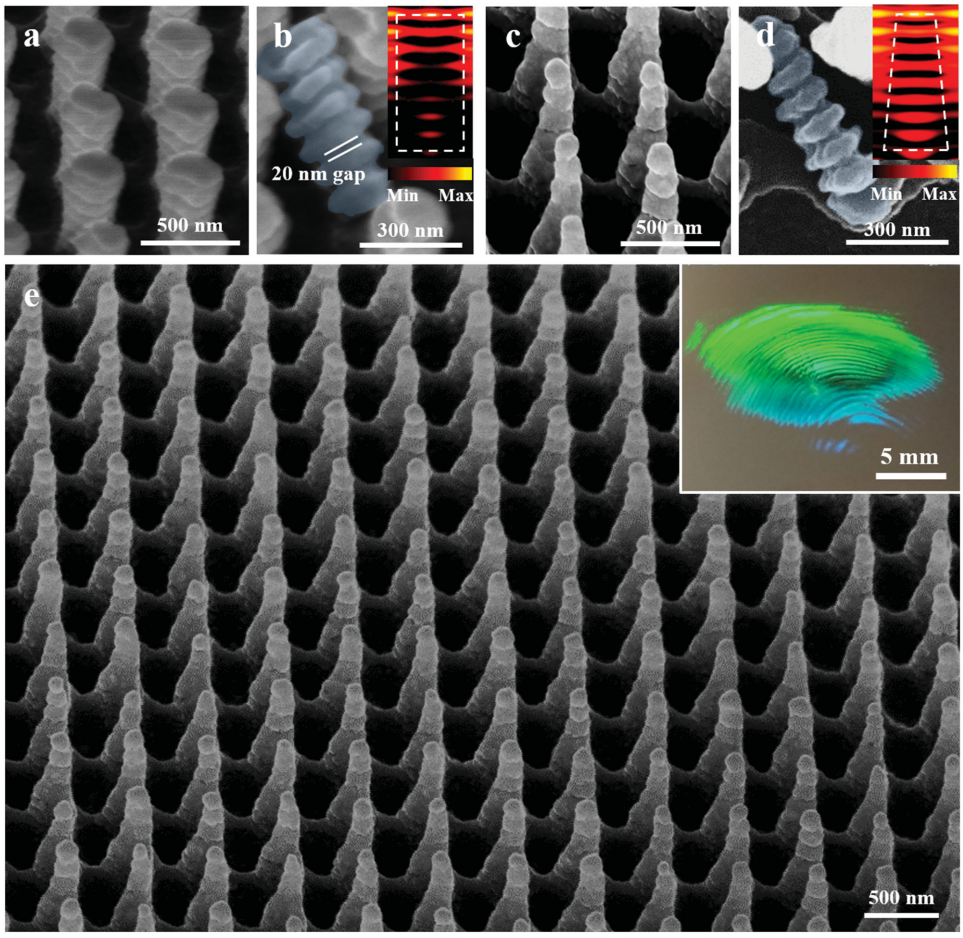

Figure 3. a,b) A set of SEM images of silver-deposited cylindrical nanopillars with 8 stories. The inset of b depicts a section of the FDTD calculation corresponding to the structure. c,d) An analogous set of data for cone-shaped nanopillars with 8 stories, where the laser dose was increased to taper the nanopillars, which is reflected in FDTD calculation (d, inset). e) Low-magnification SEM image of the cone-shaped nanopillars with 8 stories. Diffraction colors from nanopillar array are shown in the inset.

electric field is parallel to the disk. This combination of lateral and vertical coupling effects enables an electric field intensity at the nanogap ($|E_{Max}|^2$) that is approximately 1150 times larger than that of incident light ($|E_0|^2$; Figure 4c); the average enhancement of the intensity at the other nanogaps is roughly 130. In a similar manner, the EM field is more strongly coupled at the second and third nanogaps than at the others. This enhanced localization of the EM field enables higher Raman intensity in the tapered nanopillars. To quantitatively analyze the enhancement of Raman intensity, we integrated the value of $|E|^4/|E_0|^4$ along the surfaces of the three different structures (Figure S4, SI) and compared them (Figure 4d, left axis); the Raman signal is linearly proportional to the square of the electric field intensity, $|E|^4/|E_0|^4$. This trend of the integrated values of $|E|^4/|E_0|^4$ is in good accord with the experimental measurements (Figure 4b); the non-tapered nanopillars with 8 stories exhibited integrated values of $|E|^4/|E_0|^4$ that are 1.90 times those of the nanopillars with 5 stories, and the tapered nanopaillars had values 2.65 times those of the 5-story nanopillars. This confirms that high Raman intensity in the tapered structure arises as a result of the strong localization of the electric field at the narrow nanogaps.

To calculate the enhancement factor (EF) of the Raman intensity of the BT molecules by the pagoda-like nanopillars, we obtained the Raman intensities of a the monolayer of BT on the surface of the nanopillars, I_{SERS}, and of a 99% bulk BT solution, I_{Bulk}; the estimated number of BT molecules for both measurements were designated as N_{SERS} and N_{Bulk}, respectively. Because Raman intensity from one molecule on the surface of a nanopillar is I_{SERS}/N_{SERS} and that from one molecule in bulk is I_{Bulk}/N_{Bulk}, the EF can be estimated as $(I_{SERS}/N_{SERS})/(I_{Bulk}/N_{Bulk})$, where N_{SERS} is calculated from the packing density of BT molecules on a silver surface and N_{Bulk} is obtained from the bulk density of the solution (see Section S5, SI for details of the calculation). The EF values based on the Raman intensity of BT at 1071 cm^{-1} are 5.4×10^6 and 5.7×10^6 for non-tapered nanopillars with 8 and 5 stories, respectively (Figure 4d, right axis). These values are almost the same because intensities of the localized electric field at the nanogaps are comparable. In contrast, tapered nanopillars with 8 stories possess an EF twice as large, 1.05×10^7. The EF is as high as 3.15×10^8 when the top nanogap is only used to estimate the EF; this is sufficiently large for single-molecule analysis.[16] The value of $|E|^4/|E_0|^4$ for the top nanogap is 30 times the average value from the whole

© 2015 WILEY-VCH Verlag GmbH & Co. KGaA, Weinheim

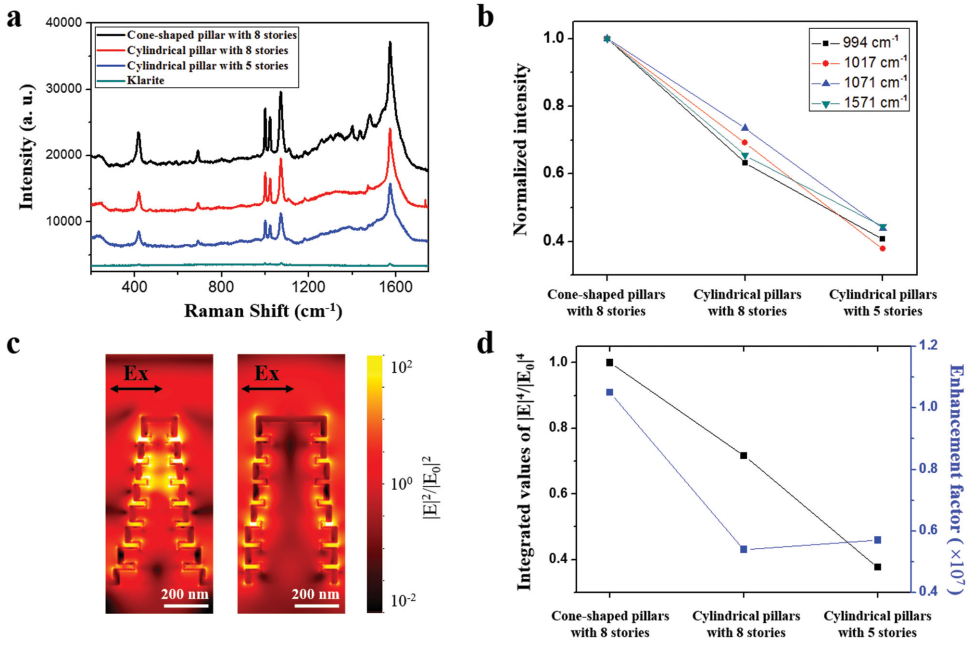

Figure 4. a) Raman spectra of BT adsorbed on the surface of cone-shaped nanopillars with 8 stories, cylindrical nanopillars with 8 stories, cylindrical nanopillars with 5 stories, and commercial Klarite substrates. b) Raman intensities at 994, 1017, 1071, and 1571 cm^{-1} for the three different nanopillar structures, where the intensities are normalized with those measured from cone-shaped ones. c) Spatial distribution of the electric field intensity, $|E|^2/|E_0|^2$, in the silver-deposited cone-shaped nanopillars (left) and cylindrical nanopillars (right). d) Integrated values of $|E|^4/|E_0|^4$ along the surfaces of the three different nanopillar structures, which are normalized with respect to that calculated from the cone-shape ones (left *y*-axis); the experimentally estimated Raman enhancement factor for the three structures (right *y*-axis).

surface (Figure S4, SI). As a result, the tapered nanopillars provide both the highest Raman intensity and EF among all three structures, making it the optimal nanopillar structure for SERS applications.

2.4. Analysis of Multiple Samples Using Micropatterned Nanopillar Arrays

We design structured nanopillar systems with two characteristic features; each nanopillar comprises multiple levels with 100-nm periodicity formed by a standing wave, and they are arranged in an array with 500-nm periodicity as a result of phase-shift interference. We can introduce an additional feature at the micrometer scale by employing photo-lithography, which is highly compatible with our current approach.[17] After laser illumination through a grating, the photoresist is further subjected to UV irradiation through a photomask. The photoresist under the transparent region of the photomask is selectively irradiated, thereby dissolving during development. For example, a photomask composed of opaque circles with transparent surroundings can be used to selectively create a pattern of circles, each with an array of pagoda-like nanopillars (**Figure 5**a,b). The circles with a diameter of 1 mm exhibit bright diffraction colors due to the formation of the regular array of nanopillars; the size of the patterns can be significantly reduced by using the appropriate photomask (Figure S6, SI).

Such micropatterned nanopillar arrays are useful for the SERS analysis of multiple samples on a single substrate. By exploiting the different wetting properties of patterned and unpatterned substrates, multiple SERS analysis is possible on a single substrate. The silver-deposited photoresist without any nanostructures shows an equilibrium contact angle of 34° for a mixture of water and ethanol at volume ratio of 3:7 (Figure S7a, SI). The same liquid spreads on the surface of the nanopillar arrays due to accommodation of the liquid in the interstices between nanopillars; this is referred to as Wenzel state.[18] The contact angle is estimated as 2° with low accuracy. As a result, the mixture prefers to wet the nanostructures rather than wet the flat surface when it is deposited on the patterns. This enables us to confine the deposited liquid on the circles of "nanopillar forests" up to a contact angle of 34°, which would otherwise spread. The surface area on which the liquid is deposited can be reduced by up to a factor of 6.88 in the circular pattern; this is with respect to the area of the unpatterned nanopillar arrays (see Figure S8, SI). Therefore, the surface concentration of molecules can be increased by the same factor, potentially providing higher intensity in the Raman signal. Superhydrophobic surfaces have been used for the concentration of an analyte to a factor of larger than 10^3;[19] however, such surfaces are not able to confine multiple independent liquid samples at a high density. To demonstrate the multiple sample analysis, we prepared four different solutions: rhodamine 6g (R6G), BT, 4-aminothiophenol (4-ATP), and 2-naphthalenethiol (2-NT). Each solution had a concentration of 2 mM and was manually deposited on four discrete circles of a patterned substrate (Figure 5c). During the evaporation of the solution, the liquid remains within its circle without spreading (Figure 5d), and the corresponding Raman spectra is obtained for the four spots, revealing the characteristic peaks of the corresponding

© 2015 WILEY-VCH Verlag GmbH & Co. KGaA, Weinheim

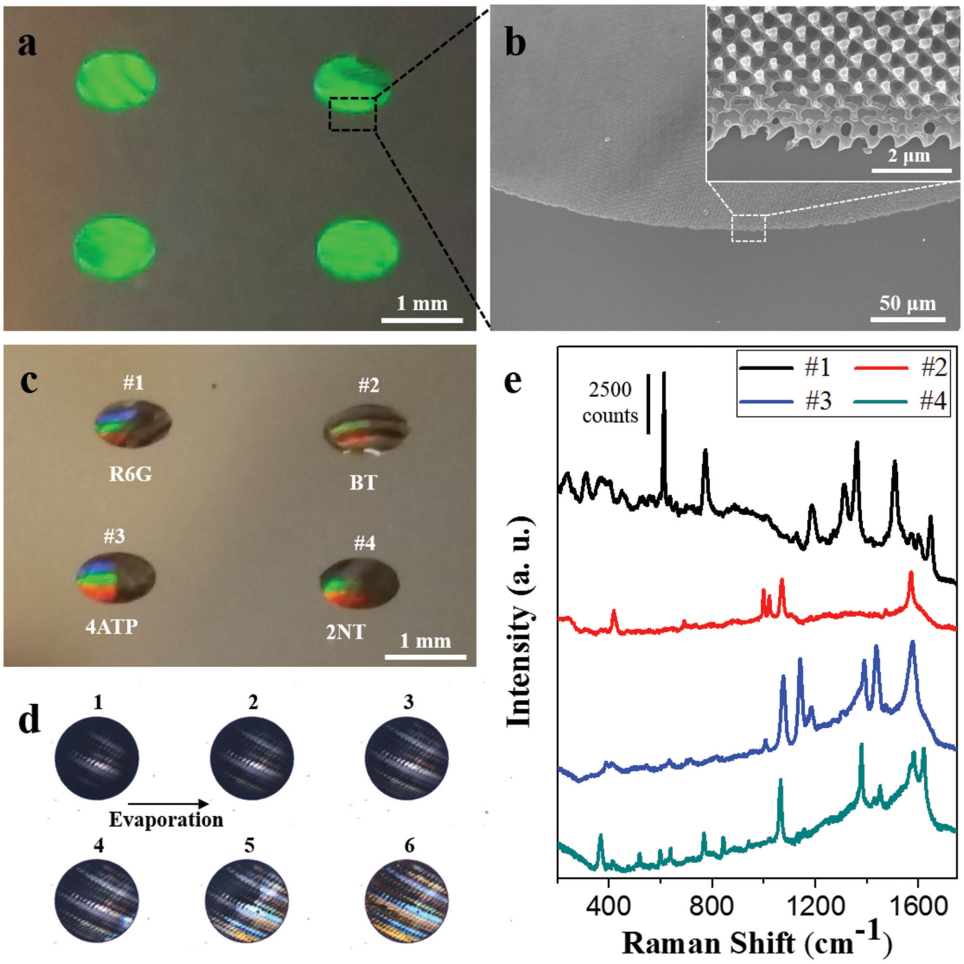

Figure 5. a) Array of circles with a diameter of 1 mm composed of silver-coated nanopillars. The circles show diffraction colors due to the periodic array of the nanopillars at the wavelength scale. b) SEM image showing the edge of a circle. The inset shows the nanopillars near the edge. c) Sample-deposited array, where four different water–ethanol solutions of rhodamine 6G (R6G), BT, 4-aminothiophenol (4-ATP), and 2-naphthalenethiol (2-NT) are dropped on circle #1, #2, #3, and #4 respectively. d) A series of optical microscopy images showing a confined drop within one of the circles during solvent evaporation. e) Raman spectra obtained from the circle #1, #2, #3, and #4 after evaporation of the solvents; the spectra show the characteristic peaks of the corresponding molecules.

molecules (Figure 5e). The density of SERS-active sites can be significantly increased by employing the micropattern of nanopillar arrays (Figure S6, SI); therefore, a micropattern of this type would be able to analyze as many as 10^4 samples per 1 cm × 1 cm if an automatic deposition system were used for the precise deposition of small amounts of samples on the active sites.

3. Conclusion

In this work, we report an optical method to create multi-dimensional structures for SERS-active substrates. Phase-shift interference was used to make periodic array of pillars at the sub-micrometer scale, and a partial standing wave was simultaneously employed to vertically integrate metal nanogaps on the side walls of the pillars; silver was used in this work, but gold could also be employed to enable long-term stability. Furthermore, photo-lithography enabled the creation of patterns of the arrays of pagoda-like nanopillars at the sub-millimeter scale, providing discrete SERS-active sites with controlled wettability. This is appealing for the analysis of many samples on a single substrate. For example, the distribution of the water pollutants of an entire lake could be analyzed using a single micropatterned substrate with high reliability by sampling water from thousands of different locations. The series of nanogaps in each nanopillar enables a high enhancement factor of the Raman signal and a large surface area for molecular adsorption. The signal can be further amplified in tapered pillars through the additional coupling of the electric field along the lateral direction. In addition, structural uniformity of the pillar array allows for a consistent Raman intensity regardless of the measurement spot position, thereby making these systems reliable SERS-active substrates. The high reproducibility, the ease of the fabrication process, and their ability for high enhancement and consistent intensity of the Raman signal will allow for these systems to provide new opportunities for practical Raman-based sensor applications.

© 2015 WILEY-VCH Verlag GmbH & Co. KGaA, Weinheim

4. Experimental Section

Fabrication of Arrays of Pagoda-Like Nanopillars: To prepare the 500-nm-thick film of positive photoresist on either soda-lime glass (Hissan) or a silicon wafer (Sehyoung Wafertech), a mixture of photoresist (AZ 5214E, Merck) and propylene glycol methyl ether acetate (PGMEA, Aldrich) at a volume ratio of 5:5 was spin-coated at 1500 rpm for 30 s and then soft-baked at 95 °C for 2 min. To prepare the 800-nm-thick film, a mixture with a volume ratio of 6:4 was spin-coated and baked under the same conditions. Optical gratings were prepared by molding PDMS hole arrays with a photocurable polymer (NOA 68, Norland Products, Inc.) to have a square array of pillars, each having a diameter of 200 nm, height of 200 nm, and periodicity of 500 nm. The grating was placed on the surface of the photoresist film with 20-μm-thick PDMS spacers; it was then vertically irradiated with a 325-nm laser with a beam diameter of 1 cm and intensity of 0.86 mW cm^{-2} (CW He-Cd laser, Kimmon) for 5 s to make non-tapered pillars and for 8 s to make tapered pillars. After the exposure, the photoresist was washed with developer (AZ 400K, Merck). Silver was deposited on the resulting pillar array using a multi-sputter (Sorona) to produce a 20-nm-thick film on the flat substrate. To pattern the nanopillar arrays, the photoresist film was irradiated through a photomask by UV light at an intensity of 14 mW cm^{-2} (CA-6M, Shinu Mst) for 30 s prior to development.

Raman Spectra: To form a monolayer of BT on the surface of the silver-coated nanopillar arrays, the substrate was immersed in an ethanolic solution of 2 mM BT for 1 h; it was then subjected to washing with ethanol and drying with nitrogen gas. To analyze four different samples using patterned pillar arrays, R6G, BT, 4ATP, and 2NT were each dissolved at a concentration of 2 mM in a mixture of water and ethanol at a volume ratio of 3:7. The samples were then dropped on the patterned system and dried at room temperature. Raman spectra from the substrate were obtained using a dispersive Raman spectrometer (Horiba Jobin Yvon) with a 1-mW, 633-nm laser and an integration time of 5 s. For Raman mapping, spectra were obtained at a power of 0.3 mW and an integration time of 1 s.

Supporting Information

Supporting Information is available from the Wiley Online Library or from the author.

Acknowledgements

This work was supported by the Fundamental Research Program (PNK 4150) of the Korean Institute of Materials Science (KIMS) and the Midcareer Researcher Program (2014R1A2A2A01005813) through the National Research Foundation (NRF) grant funded by the Ministry of Science, ICT and Future Planning (MSIP).

Received: March 30, 2015
Revised: May 15, 2015
Published online: June 22, 2015

[1] a) S. Nie, S. R. Emory, *Science* **1997**, *275*, 1102; b) R. G. Freeman, K. C. Grabar, K. J. Allison, R. M. Bright, J. A. Davis, A. P. Guthrie, M. B. Hommer, M. A. Jackson, P. C. Smith, D. G. Walter, M. J. Natan, *Science* **1995**, *267*, 1629; c) K. Kneipp, H. Kneipp, V. B. Kartha, R. Manoharan, G. Deinum, I. Itzkan, R. R. Dasari, M. S. Feld, *Phys. Rev. E* **1998**, *57*, R6281.

[2] a) R. Aroca, P. Goulet, D. Santos, R. Alvarez-Puebla, O. Oliveira, *Anal. Chem.* **2005**, *77*, 378; b) T. Y. Jeon, S.-G. Park, S. Y. Lee, H. C. Jeon, S.-M. Yang, *ACS Appl. Mater. Interfaces* **2013**, *5*, 243.

[3] a) K. Imura, H. Okamoto, M. K. Hossain, M. Kitajima, *Nano Lett.* **2006**, *6*, 2173; b) D.-K. Lim, K.-S. Jeon, J.-H. Hwang, H. Kim, S. Kwon, Y. D. Suh, J.-M. Nam, *Nat. Nanotechnol.* **2011**, *6*, 452; c) H. Im, K. C. Bantz, N. C. Lindquist, C. L. Haynes, S. H. Oh, *Nano Lett.* **2010**, *10*, 2231.

[4] a) W. Yue, Z. Wang, Y. Yang, L. Chen, A. Syed, K. Wong, X. Wang, *J. Micromech. Microeng.* **2012**, *22*, 125007; b) A. N. Grigorenko, N. W. Roberts, M. R. Dickinson, Y. Zhang, *Nat. Photonics* **2008**, *2*, 365; c) M. Chirumamilla, A. Toma, A. Gopalakrishnan, G. Das, R. P. Zaccaria, R. Karhne, E. Rondanina, M. Leoncini, C. Liberale, F. D. Angelis, E. D. Fabrizio, *Adv. Mater.* **2014**, *26*, 2353.

[5] X. Chen, H. R. Park, M. Pelton, X. Piao, N. C. Lindquist, H. Im, Y. J. Kim, J. S. Ahn, K. J. Ahn, N. Park, D. S. Kim, S.-H. Oh, *Nat. Commun.* **2013**, *4*, 2361.

[6] F. De Angelis, C. Liberale, M. L. Coluccio, G. Cojoc, E. Di Fabrizio, *Nanoscale* **2011**, *3*, 2689.

[7] a) B. K. Juluri, N. Chaturvedi, Q. Hao, M. Lu, D. Velegol, L. Jensen, T. J. Huang, *ACS Nano* **2011**, *5*, 5838; b) Y. Lu, G. L. Liu, J. Kim, Y. X. Mejia, L. P. Lee, *Nano Lett.* **2005**, *5*, 119.

[8] Y. W. Tan, J.-J. Gu, L. H. Xu, X. N. Zang, D. Liu, W. Zhang, Q. L. Liu, S. M. Zhu, H. L. Su, C. L. Feng, G. L. Fan, D. Zhang, *Adv. Funct. Mater.* **2012**, *22*, 1578.

[9] B. B. Xu, Y. L. Zhang, W. Y. Zhang, X. Q. Liu, J. N. Wang, X. L. Zhang, D. D. Zhang, H. B. Jiang, R. Zhang, H. B. Sun, *Adv. Opt. Mater.* **2013**, *1*, 56.

[10] J. Gu, W. Zhang, H. Su, T. Fan, S. Zhu, Q. Liu, D. Zhang, *Adv. Mater.* **2015**, *27*, 464.

[11] H. C. Jeon, T. Y. Jeon, T. S. Shim, S. M. Yang, *Small* **2014**, *10*, 1490.

[12] a) J. M. Kim, I. H. Cho, S. Y. Lee, H. C. Kang, R. Conley, C. Liu, A. T. Macrander, D. Y. Noh, *Opt. Express* **2010**, *18*, 24975; b)A. Isoyan, F. Jiang, Y. C. Cheng, F. Cerrina, P. Wachulak, L. Urbanski, J. Rocca, C. Menoni, M. Marconi, *J. Vac. Sci. Technol. B* **2009**, *27*, 2931; c)S. Jeon, J. U. Park, R. Cirelli, S. Yang, C. E. Heitzman, P. V. Braun, P. J. A. Kenis, J. A. Rogers, *Proc. Natl. Acad. Sci. U.S.A.* **2004**, *101*, 12428; d) T. Y. Jeon, H. C. Jeon, S. Y. Lee, T. S. Shim, J.-D. Kwon, S.-G. Park, S.-M. Yang, *Adv. Mater.* **2014**, *26*, 1422.

[13] a) H. C. Jeon, C. J. Heo, S. Y. Lee, S. G. Park, S. M. Yang, *J. Mater. Chem.* **2012**, *22*, 23650; b) C. J. Heo, S. H. Kim, S. G. Jang, S. Y. Lee, S. M. Yang, *Adv. Mater.* **2009**, *21*, 1726.

[14] H. C. Jeon, C. J. Heo, S. Y. Lee, S. M. Yang, *Adv. Funct. Mater.* **2012**, *22*, 4268.

[15] X. Zhang, Y. Zheng, X. Liu, W. Lu, J. Dai, D. Y. Lei, D. R. MacFarlane, *Adv. Mater.* **2015**, *27*, 1090.

[16] E. C. Le Ru, E. Blackie, M. Meyer, P. G. Etchegion, *J. Phys. Chem. C* **2007**, *111*, 13794.

[17] a) A. M. Bowen, M. J. Motala, J. M. Lucas, S. Gupta, A. J. Baca, A. Mihi, A. P. Alivisatos, P. V. Braun, R. G. Nuzzo, *Adv. Funct. Mater.* **2012**, *22*, 2927; b) S. K. Lee, S. G. Park, J. H. Moon, S. M. Yang, *Lab Chip* **2008**, *8*, 388.

[18] P. S. H. Forsberg, C. Priest, M. Brinkmann, R. Sedev, J. Ralston, *Langmuir* **2010**, *26*, 860.

[19] F. Gentile, M. L. Coluccio, N. Coppedè, F. Mecarini, G. Das, C. Liberale, L. Tirinato, M. Leoncini, G. Perozziello, P. Candeloro, F. De Angelis, E. Di Fabrizio, *ACS Appl. Mater. Interfaces* **2012**, *4*, 3213.

© 2015 WILEY-VCH Verlag GmbH & Co. KGaA, Weinheim